IEEE Access
Multidisciplinary | Rapid Review | Open Access Journal

Received July 18, 2020, accepted July 31, 2020, date of publication August 4, 2020, date of current version August 25, 2020.

Digital Object Identifier 10.1109/ACCESS.2020.3014249

ADS-B Based Wind Speed Vector Inversion Algorithm

TAO LIU[1,2], TAISONG XIONG[3], LENWORTH THOMAS[4], AND YONGLOU LIANG[5]

[1]School of Electronic Engineering, Chengdu University of Information Technology, Chengdu 610225, China
[2]CMA Key Laboratory of Atmospheric Sounding-KLAS, Chengdu 610225, China
[3]School of Applied Mathematics, Chengdu University of Information Technology, Chengdu 610225, China
[4]Department of Mechanical and Aerospace Engineering, University of Florida, Gainesville, FL 32603, USA
[5]Beijing Huayun Shinetek Science and Technology Company, Beijing 100089, China

Corresponding author: Taisong Xiong (xts@cuit.edu.cn)

This work was supported by the Sichuan Science and Technology Program under Grant 2018RZ0072.

ABSTRACT Besides collecting and broadcasting aviation surveillance parameters, Automatic Dependent Surveillance-Broadcast (ADS-B) is also a novel technique to sense and share meteorological information such as wind field with high update rate and accuracy. Many ADS-B devices on aircraft can construct a real-time and dynamic sensor network. Although the ADS-B message format reserves the items especially for wind information, few aircrafts broadcast these items at present. The current solution is to use the aircraft trajectory captured by ADS-B for wind vector inversion. Nevertheless, some algorithms still have some downsides, especially the stability in small-angle turning situations. This article is committed to developing a novel algorithm capable of working in both small and large angle turning situations with high efficiency, with an emphasis on small angle situations. By virtue of the algorithm in our recent research which is derived from the Particle Filter model, this algorithm takes advantage of circle geometry property and Euclidean distance standard deviation (STD). In the simulation test, the effect of true airspeed (TAS) difference on the mean absolute error of wind estimate, the effect of true wind speed on wind estimate, the effect of maneuver turning angle on wind estimate, and the computational complexity are assessed, respectively. Moreover, for real ADS-B data, both large and small-angle turning maneuver situations are tested and compared separately. Also compared is the level of the results concentration for the wind speed and TAS along with the geometric height. Consequently, the simulation and the real data test shows that the proposed STD algorithm has performance superior to other two algorithms LS and LM especially in the small-angle turning situation such as below 40deg. STD's performance is between other two algorithms in computational complexity. This property can help improve the algorithm's stability and data utilization for small-angle turning significantly, which is very useful in real aviation surveillance operations.

INDEX TERMS Automatic dependent surveillance-broadcast (ADS-B), wind vector inversion, turning maneuver.

I. INTRODUCTION

In daily operations, meteorology and aviation are inseparable because aviation is sensitive to common meteorological factors such as wind, humidity, and air pressure. According to existing research [1], wind can more often influence flight trajectory and estimated arrival time even for daily flight. Extreme weather phenomena, including strong winds, dense fog, and heavy snow, will strongly and directly affect flight operation or lead to flight delays, or, worse, lead to safety accidents. Among these meteorology factors, wind shear ranks the most common and dangerous one because of its invisibility to naked eyes, occurrence whenever and wherever possible, rapid change, and low predictability. Downwind shear, headwind shear, vertical wind shear, and lateral wind shear significantly affect the lift, balance, and attitude of the aircraft. They seriously threaten the flight safety during low altitude flight, approaching, landing and take-off. Therefore, real-time detection of wind field information in aviation and early warning of wind field shear change through atmospheric detection system are two essential factors concerning aviation and airport safety operation. Thus, the topic of mitigating

The associate editor coordinating the review of this manuscript and approving it for publication was Wei-Wen Hu.

these issues is of high priority in aviation meteorological research.

In general, the real-time and spatial-temporal resolution requirements for aviation weather information are relatively high, unlike conventional weather detection. Conventional wind field detection methods and equipment have various defects and difficulties in the field of aviation meteorology. First of all, the wind profile radar can only detect vertically or with a large elevation angle, and its horizontal resolution is relatively low [2]. Another downside is that the echo signal-to-noise ratio (SNR) is low and vulnerable to noise. Secondly, the detection of Doppler radar depends heavily upon reflection of precipitation particles floating in the air. So, the lack or absence of precipitation particles will significantly hinder the performance. Thirdly, the LiDAR must operate in clear sky conditions; that is to say, fog, rain, and sandstorm will affect and even disable its detection ability [3]. Next, the radio sounding balloon has a low daily flying count in daily routine (typically twice per day), and its flying station distribution in a large area is geographically uneven [4]. Furthermore, for the multi-radar system, the beam overlap region is limited, and the inversion algorithms are more complicated than that of single-radar. The cooperation and synchronization between separate radars remain challenging currently. High cost of multi-radar also limits its deployment [5]. These downsides mentioned above significantly affect the broad application of traditional wind field detection methods in airport meteorological services [6].

Automatic Dependent Surveillance-Broadcast (ADS-B) [7] is a kind of novel sensor network for meteorological information. Originally, ADS-B is deployed as a sort of up-to-data aviation surveillance technology and currently operating worldwide [8]. Airborne aircraft equipped with ADS-B device can continuously sense their aviation parameters (such as position, altitude, and speed) [9], then broadcast these messages via a public and unencrypted data chain to nearby aircraft and ground stations automatically. Unlike the interrogation-reply model in secondary surveillance radar (SSR) [10], ADS-B operates automatically and continuously without interrogation, with an update rate up to 1-2Hz. Some open or commercial websites, such as Flightradar24, adopt ADS-B as their data source. Currently, most attention and research are focused on the hardware devices [11], radio signal processing [12], [13], ADS-B network [8], and aviation surveillance [14]. Besides typical aviation parameters, some meteorological parameters such as wind, temperature, pressure, and humidity will be captured in real-time and broadcasted along with other flight data. Nearby aircraft can share local meteorological information; on the other hand, on-ground air traffic control (ATC) can reconstruct the meteorological field of the entire surveillance airspace. There are many reasons why the wind field information acquisition method specifically based on ADS-B technology has drawn more and more attention from researchers and specialists, including high data update rate and high cost-performance ratio. ATC and nearby aircraft can obtain the full wind and other meteorological information for such interesting area as flight route and airport with high spatial-temporal sampling frequency and resolution. Furthermore, the system upgrade cost is relatively low because ADS-B systems for aviation surveillance have been deployed and operating for many years. These features and merits have motivated more research on ADS-B-related meteorological parameters acquisition and application, such as airspace extreme weather surveillance and warning system [15].

In 1989, Hollister proposed a novel method to estimate wind vector aloft using aircraft radar track [16]. Although his remote-sensing equipment is radar, the rationale is feasible for ADS-B data. In 2009, Delahaye developed a linear model and utilized Kalman Filter to obtain wind estimates with high quality. He concluded that the wind vector might be inverted only if aircraft trajectories have one or two turn maneuvers depending on the number of aircraft in the interesting area. Based on these conditions, closed forms of the wind speed had been developed for the one and two aircraft cases, respectively. All these principles and algorithms can be extended to ADS-B cases [17].

In 2013, Haan studied the wind and temperature observation method [18], where he synchronized SSR and ADS-B data. In the same year, Leege conducted studies on the wind vector solution of single and multiple aircraft ADS-B equipment [19], assuming that the aircrafts among specific spatial area have approximately the same TAS with uniform distribution in each direction. Thus, the wind vector and TAS inversion are modeled as the circle fitting problem and nonlinear Least-Square problem, followed by the extended Kalman Filter (EKF) to filter out noise. The vertical wind profile results were compared with forecasts from the GFS numeric weather prediction model ran by the National Oceanic and Atmospheric Administration, achieving the performance of mean absolute error (MAE) between the forecasts and estimates about 9.5 kt. In 2014, Liou used the ADS-B data provided by the AMDAR system as well as other meteorological data (such as ground station data), and then fed them into the CALMET numerical prediction model for spatial 3D fluid wind field reconstruction. He verified his system based on data around the Taiwan area [20]. In 2014, Kapoor studied the feasibility of weather observation by sensors mounted on commercial aircraft at the continental scale. A novel stochastic model based on the Gaussian processes was adopted to merge the airborne aircraft observations and ground station observations. He focused on the problem of forecasting and used machine-learning methods. The learned predictive model was verified with data from an instrumented high-altitude balloon [21]. In 2014, Hurter proposed a linear algorithm for the wind vector inversion from the turning maneuver clips. He simplified the original two-order signal model by inferring the triangular and projection relations and ignoring some items. Next, it uses the Least Square for the final solution [22]. In 2017, Ting used ADS-B data to establish a software system for nowcasting of unusual weather [23]. The experimental data were derived from a 1090MHz Mode-S ES transponder with an

update rate of 1Hz. Based on the wind speed components, the Richardson number was derived as the key parameter for now-casting. In 2017 and 2018, Sun studied the wind and temperature field reconstruction for upper airspace and proposed a novel meteo-particle model based on the Gaussian random walk model [24], [25]. In 2018, Huy combined ADS-B and Mode-S data to retrieve the wind field [26]. He meticulously analyzed and explained the difference in how to retrieve TAS from both systems. From 2016 to 2018, Matthias Schafer and his team continuously issued the up-to-date fruits of their research on ADS-B and SSR. The reports provided the up-to-date statistics on SSR Mode S and 1090ES ADS-B utilization on both military and civil aviation from the OpenSky Network [27]–[29].

For the spatial 3D or spatial-temporal 4D wind reconstruction in the large area and subsequent forecast, the modeling and inversion of wind vector in a specific space point is the fundamental task. Although ADS-B standards reserved the items for wind speed vector, meteorological information, true airspeed, indicated airspeed and Mach number, as designed in Category 21 [30], few airborne ADS-B devices currently broadcast this information. There are two leading solutions in the existing literature to wind vector acquisition: those based on combining both ADS-B and SSR Mode-S messages and those based on ADS-B trajectories and ground speed. If there are no SSR Mode-S interrogation-reply messages, the wind speed vector can only be derived by trajectories during a short period from ADS-B messages, only when the aircraft is making a turning maneuver.

From 2019, we studied some fundamental issues on: 1) the raw ADS-B dataset coding procedure and programming, directly from the ADS-B network instead of uniform data service platforms such as OpenSky and AMDAR; 2) the wind vector inversion algorithm and real data experiments testing. Particular issues such as message format and key fields are discussed in the article [6]. During the research, we found that some sample clips with smaller turning angles below 40deg would cause wrong results with higher probability than large angle turning cases. In 2020, we proposed a particle filter method for wind vector inversion and achieved an attractive achievement, especially in small-angle turning maneuver cases [31]. Nevertheless, this one still had the downside of high computational complexity; specifically, the computational complexity will exponentially decrease along with the particle number increasing. This article and related research will focus on exploring a new inversion algorithm with low computational complexity, and meanwhile, it can effectively work at small-angle turning.

This article will focus on the technical details of single wind vector inversion algorithms only from the ADS-B trajectories without Mode-S. A typical signal model is introduced in section II, followed by several algorithms of previous scholars and the new method proposed in this article. Also introduced are the hypotheses of wind constant and the TAS remaining constant. In section III, the simulation tests are conducted to compare the performance of three algorithms and verify various effects posing on the estimate. In section IV, actual ADS-B data from ATC are applied to these algorithms to compare the stability and other factors. The cases of large and small angle turning maneuvers are also tested, respectively. In Section V, we present our conclusions and main takeaways.

II. RELATED WORK

A. SPEED VECTOR MODEL

First of all, one crucial question must be mentioned: although Category 21 has reserved items (I021/220 Subfield #1 and #2) for wind speed vector [30], it is unavailable currently; more specifically, few aircraft broadcast this item. Therefore, we can only derive wind speed indirectly by virtue of the speed vector model comprising the ground speed vector and the TAS vector.

Deriving from the schematics of the kinematics of airplanes encountering a horizontal wind described in [32], during the descent or climbing phase, the flight-path angle is rather small, causing the velocity component of aircraft to be the largest one in the horizontal plane. From this point of view, the speed model can be simplified to comprising only TAS, ground speed, and wind speed in the horizontal plane by neglecting vertical components. From this point onward, speed vectors and signal models are only considered in the horizontal plane in our research.

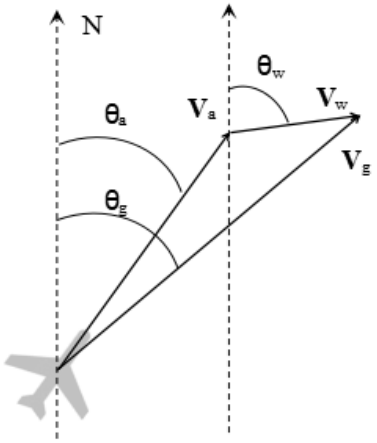

FIGURE 1. Vector relation of ground speed, airspeed, and wind speed.

In the horizontal plane, the ground speed vector is the sum of the wind speed vector and airspeed vector, whose triangular relation is depicted in Figure 1, and the mathematical model is denoted in (1).

$$\mathbf{V}_g = \mathbf{V}_a + \mathbf{V}_w \tag{1}$$

where $\mathbf{V}_g$ is the ground speed vector and its angle is θ_g; $\mathbf{V}_w$ is the wind speed vector and its angle is θ_w; $\mathbf{V}_a$ is the airspeed or the true airspeed instead of the indicated airspeed or Mach number, and its angle is θ_a. Based on the aviation principle, 0 degrees for any vector points to the true north. The angle degree increases along clockwise. When there is no wind,

aircraft will fly exactly along the desired heading angle, and TAS equals the ground speed. When there exists wind with a certain angle (not 0 or 180 degrees), aircraft will drift from the desired or planned trajectory, or the actual flying direction will be away from the heading angle.

Mathematically, the wind speed vector can be figured out when subtracting the ground speed vector to the TAS vector. The ground speed vector is measured by means of the Global Navigation Satellite System or Inertial Reference Unit. The TAS amplitude is determined using the Air Data Computer and pitot-static system for input of impact pressure, static pressure, and total air temperature [32]. The TAS angle is determined by the Magnetic Heading item. In the ADS-B OUT message, based on the Category 21 [30] format partially shown in Table 1, three speed vectors can be retrieved directly.

TABLE 1. Speed vector related definition in CAT21.

FRN	Data Item	Information
10	I021/151	True Air Speed
22	I021/152	Magnetic Heading
26	I021/160	Airborne Ground Vector
31	I021/220	Met Information (comprising wind speed vector)

However, in the real situation, neither TAS (I021/151) nor Magnetic Heading (I021/152) is available in ADS-B messages. Currently, few airborne aircraft send out TAS items. Therefore, it is challenging to retrieve the wind speed vector from (1).

In the previous research, some hypotheses are proposed to simplify (1) for the trajectory within a local spatial-temporal grid (4D-grid):

1) the wind speed vector remains nearly constant

2) aircraft have the same TAS but different track angle, especially for single turning trajectory

For simplicity, we initially focus on the wind inversion for the single aircraft. The same model and algorithm can be extended to multiple aircraft situations.

After decomposed, speed vectors give the north-south components and the east-west components:

$$V_{ax} = V_{gx} - V_{wx} \tag{2}$$

$$V_{ay} = V_{gy} - V_{wy} \tag{3}$$

where the north-south and east-west components are denoted by x-subscript and y-subscript, respectively. Thus, we construct a 2D speed state space consisting of two speed components. Figure 2 depicts an example of speed state space, dotted in blue by the north-south and east-west components of the ground speed of a single aircraft flying horizontally with approximately 70deg turning maneuver. These points

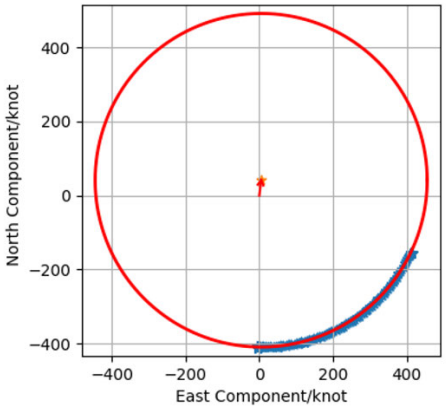

FIGURE 2. An example of ground speed points, fitted circle, and center in speed state space from real ADS-B message.

approximate a circle (red) in state space, given by the circle equation in (4).

$$\|V_a\|^2 = \left(V_{gx} - V_{wx}\right)^2 + \left(V_{gy} - V_{wy}\right)^2 \tag{4}$$

The circle center (in yellow) offset from the origin, corresponds to the wind speed vector, denoted as $\left(V_{wx}, V_{wy}\right)$. The circle radius is determined by TAS, denoted as $\|V_a\|$. Ground speed samples are dotted around the circle edge. From this point of view, the wind vector inversion problem is transferred to a circle fitting problem with unknown center $\left(V_{wx}, V_{wy}\right)$ and radius TAS from the known ground speed points (blue points). When the aircraft flies straightly, all ground speed points in the state space will locate in a single position, and the circle can never be fitted. When the aircraft makes a turning maneuver, ground speed points will separate along the circle edge. The more the aircraft turns, the more the points separate, and the easer the circle can be fitted. Although Hough Transform is a typical fitting algorithm for circle, especially in the research of digital image processing, it is not suitable here because of insufficient points around the circle, and of the high computational complexity. Based on this model, three algorithms are introduced below.

B. NONLINEAR LEAST SQUARES

Leege proposed a loss function for N observations of one aircraft with large turning maneuver in (5)

$$S = \sum_{i=1}^{N} \left(\left(V_{gxi} - V_{wx}\right)^2 + \left(V_{gyi} - V_{wy}\right)^2 - \|V_a\|^2 \right) \tag{5}$$

The optimization techniques can be applied to minimize the above nonlinear Least Squares problem. Leege adopted the Levenberg-Marquardt algorithm to solve the unknown parameters of wind speed and TAS in (5). Later in 2013, Leege used another modified extended Kalman filter algorithm to solve the nonlinear optimization problem [19]. Both algorithms have almost the same final iteration error. From this point onward, this algorithm proposed by Leege is denoted as symbol LM for the discussion in the next section.

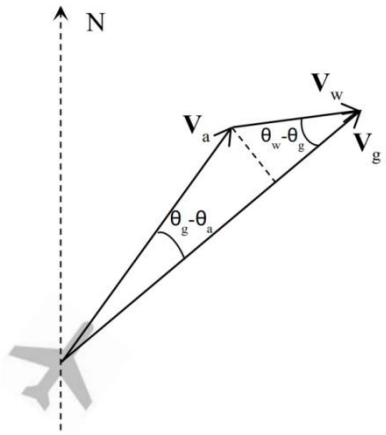

FIGURE 3. Projection along the ground speed direction.

C. LINEAR LEAST SQUARES

In 2014, Hurter proposed a linear model for simplicity [22]. With projection along the ground speed vector direction, as shown in Figure 3, the amplitude of the ground speed vector gives:

$$\|\boldsymbol{V}_g\| = V_g = V_a cos(\theta_g - \theta_a) + V_w cos(\theta_w - \theta_g) \quad (6)$$

where $(\theta_g - \theta_a)$ is the drift angle, typically rather small. For example, during the cruising phase with the TAS 560 knots and the vertical wind of 50 knots, we get

$$cos(\theta_g - \theta_a) \approx 0.9960 \approx 1 \quad (7)$$

So, the above (7) can be simplified as

$$V_g = V_a + V_w cos(\theta_w - \theta_g) \quad (8)$$

or $V_g = V_a + V_w(cos\theta_w cos\theta_g + sin\theta_w sin\theta_g)$

When denoting

$$V_{wx} = V_w sin\theta_w \quad (9)$$

$$V_{wy} = V_w cos\theta_w \quad (10)$$

then we get

$$V_g = V_a + V_{wx} cos\theta_g + V_{wy} sin\theta_g \quad (11)$$

For i-th ground speed,

$$V_{gi} = V_a + V_{wx} cos\theta_{gi} + V_{wy} sin\theta_{gi} \quad (12)$$

where V_{gi} and θ_{gi} can be directly achieved from the ADS-B message, and the above equation is linear with respect to V_a, V_{wy} and V_{wx}. Considering K measurements $\left\{\left(V_{gi}, \theta_{gi}\right)\right\}_K$ and ground speed θ_{gi}, we get

$$AV = b \quad (13)$$

$$b = \left[V_{g1}, \ldots, V_{gK}\right]^T \quad (14)$$

$$A = \begin{bmatrix} cos\theta_{g1} & sin\theta_{gK} & 1 \\ \vdots & \vdots & \\ cos\theta_{gK} & sin\theta_{gK} & 1 \end{bmatrix} \quad (15)$$

$$V = \begin{bmatrix} V_{wx} & V_{wy} & V_a \end{bmatrix}^T \quad (16)$$

In general, the measurement count N is much greater than the number of unknown variables (here it is 3), or matrix A is of full-column rank. So (13) is over-determined. The least-squares minimum norm solution gives:

$$\tilde{V} = (A^T A)^{-1} A^T b \quad (17)$$

Finally, the wind speed and direction are obtained using the following equations,

$$V_w = \sqrt{V_{wx}^2 + V_{wy}^2} \quad (18)$$

$$\theta_w = arctan\frac{V_{wy}}{V_{wx}} \quad (19)$$

From this point onward, this algorithm proposed by Hurter *et al.* [22] is denoted as symbol LS.

D. STANDARD DEVIATION BASED ALGORITHM

Recently in our relative research, we proposed a novel Particle Filter (PF) algorithm for wind speed vector inversion [31]. PF Particle Filter is a typical algorithm derived from the Bayesian filter and the Monte Carlo sequence sampling to estimate the posterior expectation through multiple iteration steps

$$\hat{x}_k^{MMSE} = \mathbf{E}[f(x_k)|Y_k] = \int f(x_k) p(x_k|Y_k) dx_k \quad (20)$$

The 2D speed state space is still based on the wind speed vector model and hypothesis mentioned above. The key point is that in the prediction phase, the similarity metric for the i-th particle is defined as the variance of distance values between every ground speed to the i-th particle, as shown in (21). That is to say, particles closer to the circle center indicated by the true wind speed will have a smaller variance.

$$var\left(d_i(x, y)\right) = var\left\{d\left(p_i, w_{gk}\right), k = 1, 2 \ldots P\right\} \quad (21)$$

where $d\left(p_i, w_{gk}\right)$ is the Euclidean distance between i-th particle state(speed) and the k-th ground speed. P is the number of ground speed samples. This algorithm obtained better results especially in smaller angle turning, at least without obvious incorrect results such as wind speed estimate above 200 knots [31].

Nevertheless, after wide application, this algorithm revealed the downside of higher computational complexity, which is sometimes intolerable if the ground speed samples numbers were over 100. To solve this problem, by analyzing on its properties and merits, a new, faster algorithm with better performance is proposed in this article. The x and y components of the wind vector in the state space is estimated by minimizing the standard-deviation-based loss function below:

$$(x, y) = \underset{(xy)}{\text{argmin}}\ std\left\{d_i(x, y), i = 1, 2, \cdots N\right\} \quad (22)$$

where $d_i(x, y)$ is the Euclidean distance between the point (x,y) and the i-th ground speed point. Operator $std\{S\}$ represents the standard deviation calculation on set $\{S\}$. Moreover, N is the number of ground speed samples.

Some typical optimum algorithms can be used to iteratively solve the wind speed component (x,y). in our experiments, the Sequential Least SQuares Programming optimization algorithm (SLSQP) is adopted. SLSQP is already embedded in the SciPy package of Python. SciPy is a fundamental package for scientific computing such as mathematics, science, and engineering, and is very popular in the Python developing society. Specifically, we use the optimization function *minimize*( ) in the *scipy.optimize* package and set the parameter method = 'SLSQP'. After that, through (18) and (19), the wind vector can be obtained. This algorithm makes full use of the shape features of the circle: the radii from the circle center will have the minimum standard deviation even with certain noise. This new algorithm has almost the same performance as that of the LM and LS algorithm in larger flight turning situations. Furthermore, it has higher stability and superiority over the other two in case of aircraft small turning maneuvers, as demonstrated in the next sections. From this point onward, this new proposed standard-deviation-based algorithm is denoted as the symbol STD.

In the case of multi-aircraft located in the local spatial-temporal grid, assume that wind speed and direction remain constant, whereas the TAS difference between aircraft cannot be ignored. Aircraft ground speed data with different TAS may be regarded as being contaminated by noise and may degrade the performance of the inversion algorithm. So, data from different aircraft cannot be fed into one set for the *std* operator in (22). A modified version of the loss function is shown in (23)

$$(x, y) = \underset{(xy)}{\operatorname{argmin}} \sum_{m=1}^{M} std\left\{d_i\left(x, y\right), i = 1, 2, \cdots N_m\right\} \tag{23}$$

where M is the aircraft amount; N_m is the ground speed samples amount for m-th aircraft.

III. SIMULATION STUDY

In this article, we adopt two datasets: one from the simulation platform and the other from the Civil Aviation Gansu Air Traffic Control Sub Bureau. The simulation study is conducted to assess and compare the performance of the above-mentioned algorithms with respect to the true value. Table 2 lists the factors varying to generate the simulation conditions. There are 1000 data points in each simulation. Here we ignore the flight level (FL) and geometric height factor but equivalently focus on the TAS difference influence on the estimate, which may primarily be caused by height descent or ascent.

A. EFFECT OF TAS DIFFERENCE ON MEAN ABSOLUTE ERROR OF WIND ESTIMATE

Firstly, we assess the effect of TAS difference on MAE of wind estimate for all algorithms, as shown in Figure 4 and 5. The error bar is for 95% confidence interval (CI). In both figures, the x-axis represents the standard deviation of TAS, meaning TAS difference; the y-axis shows the estimate MAE

TABLE 2. Simulation factors.

Factors	Values
Data points	10,30,50
TAS	Normally distributed with mean 400 knots and standard deviation a=5,10,15...55 knots
Track angle	Uniformly distributed between 0 and span, where span=45,90,135,…360deg
Wind speed	Uniformly distributed between 25 and 70 knots
Wind angle	Uniformly distributed between 0 and 360 degrees

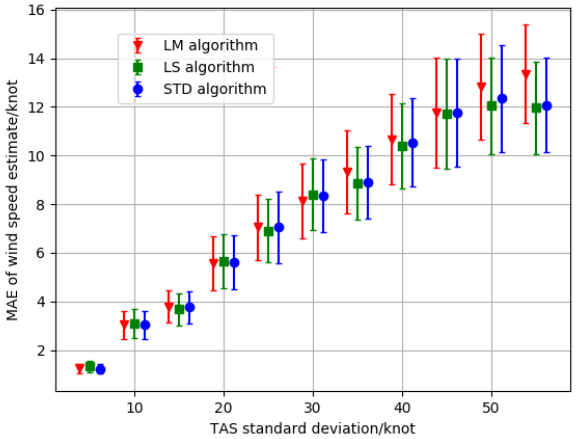

FIGURE 4. Effect of TAS difference on MAE of wind speed estimate (95% CI).

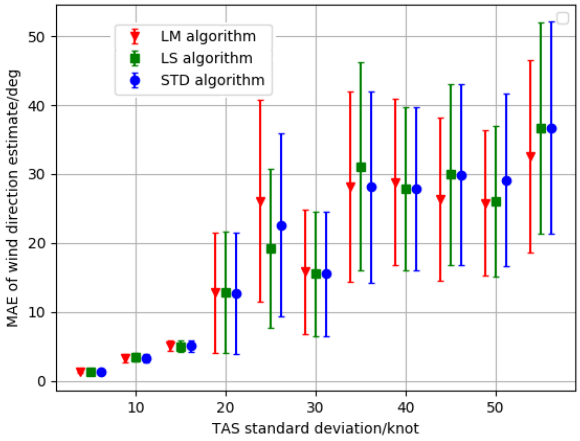

FIGURE 5. Effect of TAS difference on MAE of wind direction estimate (95% CI).

of wind speed and direction, respectively in two figures. In the simulation, the TAS mean is set to 400 knots, approximately 90% cruising speed of a midsized jet like the Boeing 737-800. MAEs for all three algorithms are depicted at every standard deviation value in this figure to compare the performance in the same situation.

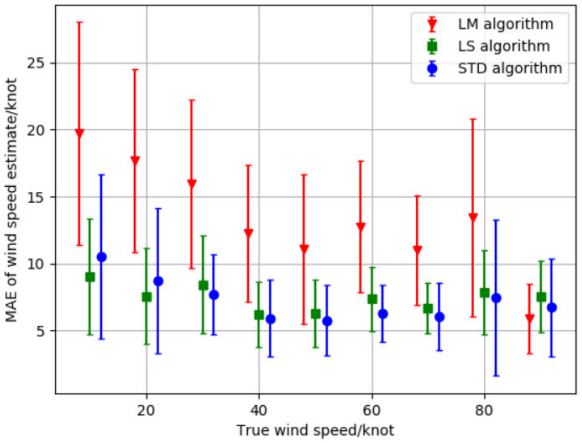

FIGURE 6. Correlation between MAE of wind speed estimate and true wind speed (95% CI).

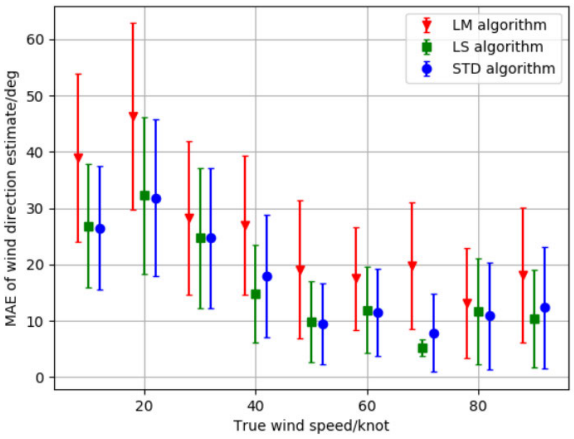

FIGURE 7. Correlation between MAE of winddirection estimate and true wind direction (95% CI).

It can be seen from Figure 4 and 5 that both wind speed and direction estimates are negatively affected by TAS difference or standard deviation. If 95% of the aircraft operate within 15 knots of airspeed, MAE of 1-4 knots and 1-5deg for the wind speed and direction estimates are expected, respectively.

It is evident that in Figure 5 the wind direction estimate is more sensitive to errors than the wind speed because the wind direction is synthesized from both east-west and north-south components of the wind speed vector. Smaller changes in any component will cause a relatively larger angle varying but smaller amplitude varying in case of lower wind speeds [19]. Also, the three algorithms have almost the same performance along with TAS standard derivation increasing.

B. EFFECT OF TRUE WIND SPEED ON WIND ESTIMATE

Figure 6 and 7 illustrate the relation between the true wind speed and MAE of wind speed and direction, respectively. In both figures, MAEs of LM are higher than those of LS and STD. Table 3 specifically lists the R and p values for both figures and all three algorithms. It is clear that the MAE of wind speed estimate is uncorrelated with the actual wind speed for LS and STD algorithms, $p > 0.01$. For all three algorithms, MAEs of wind direction estimates are negatively correlated with the actual wind speed, $|R| > 0.8$ and $p < 0.01$. This correlation trend can also be seen in Figure 7. Furthermore, LS and STD have closer MAE performance, both apparently less than that of LM.

TABLE 3. R and p values for wind estimates.

Item	Method	R	p
Wind speed	LM	-0.8643	0.0027
	LS	-0.3676	0.3305
	STD	-0.6374	0.0648
Wind direction	LM	-0.8680	0.0024
	LS	-0.8387	0.0047
	STD	-0.8419	0.0044

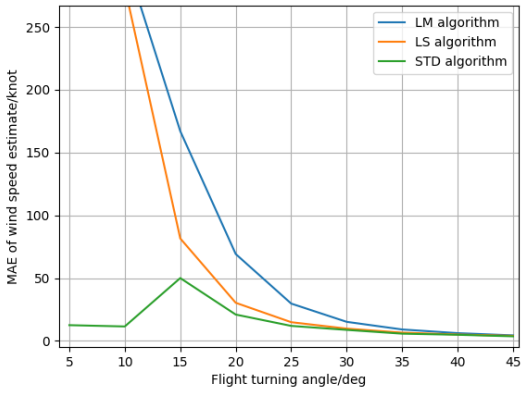

FIGURE 8. Effect of turning angle on MAE of wind speed estimate.

C. EFFECT OF MANEUVER TURNING ANGLE ON WIND ESTIMATE

In this simulation, the conditions are a little different from that in Table 2. The TAS standard deviation constantly remains 2 knots. In every test, the minimum angle of ground speed pointed around the circle edge is uniformly and randomly selected between 0 to 360deg, starting from which N simulation samples of ground speed with 1-degree interval were generated. Therefore, the simulation sample number corresponds to the maneuver turning angle span in our simulation.

The geometry of the circle will influence the quality of the wind estimate. Thus, data points with a larger angle span or turning maneuver angle in speed state space are likely to generate a better estimate than those points with a smaller angle span. This influence is fully demonstrated in Figure 8 and 9, in which we can observe that the geometry or the sample

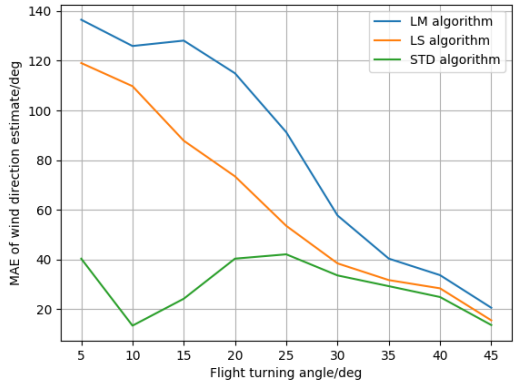

FIGURE 9. Effect of turning angle on MAE of wind direction estimate.

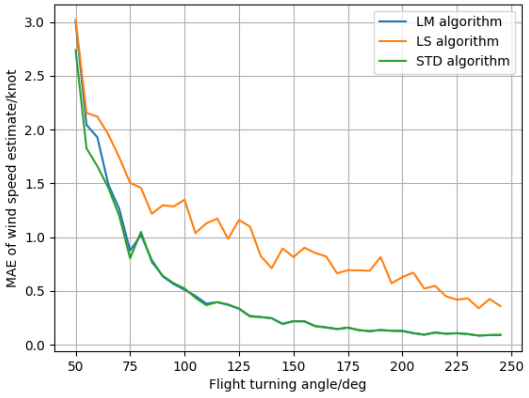

FIGURE 10. MAE convergence over 50deg.

number has positive affection on the estimate of wind speed and direction. In Leege's article [19], this influence was also mentioned, but without verification with simulation and real data. Our experimental result and conclusion agree with the viewpoint of Leege.

In this section, we verify this influence and compare the performance, especially in the small turning angle. Above 30deg, all algorithms have almost the same MAE performance of wind speed. When under 30deg, MAE of LM and LS will increase suddenly with the decrease of angle span. Especially under 20deg, LS has such unsatisfactory performance that it can't be applied to real situations. However, STD remains very low MAE, which shows the superior performance in comparison to the other two algorithms. By this merit, we can further use the turning trajectory under 30deg and increase the data availability. This superiority can also be shown in our real data experiments.

Considering turning over 50deg, as shown in Figure 10. With the turning angle increasing over 220deg, all three algorithms will converge to satisfactory MAE values under 0.5 knots. Furthermore, LM and STD have a slightly better MAE convergence property superior to LS, about 1/3 of MAE value of the latter. All three algorithms have satisfactory performance in the large angle turning maneuver situations. Again, it is concluded that the geometry of the turning angle has a positive influence on the MAE performance.

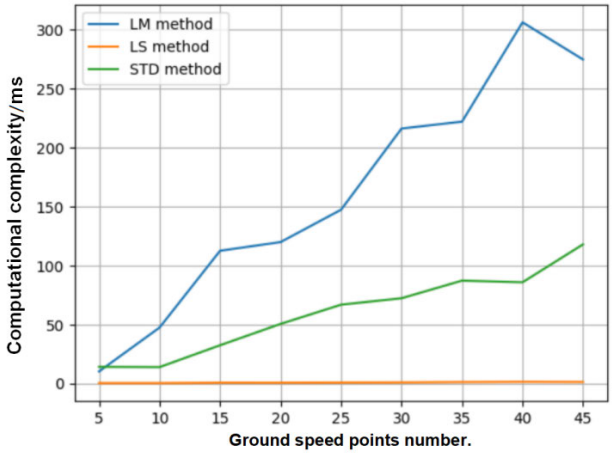

FIGURE 11. Computational complexity vs ground speed points number.

D. COMPUTATIONAL COMPLEXITY

This experiment compares the computational complexity vs. the number of ground speed samples among three algorithms, and Figure 11 shows the results. Here, the computational complexity is defined as the time consumption of every algorithm in specific sample counts of ground speed. We use Monte Carlo method to simulate 1000 cases of computation in every sample count, accumulate the total time consumption, and divided by 1000 to obtain the consumption for every case and every algorithm. In our experiment, we use the following hardware specification: CPU I7;8G Mem; 128G SSD; no hardware speedup. The millisecond value of y-axis will vary in different hardware platforms. Our concentration is not the exact values but the comparisons among the three algorithms.

In the result, LS has the lowest computational complexity, almost remaining constant even with the number increasing. Because the LS model is linear, the complexity will not increase significantly along with the points number.

Both for LM and STD, the computational complexity has a strong positive correlation with the points number. The reason is that both LM and STD are nonlinear models, and the square calculations amount equals the number of ground speed samples; that is to say, the model complexity strongly depends on the points number. Furthermore, it can be seen in Figure 11 that STD has approximately 1/3 of the time consumption of that of LM.

Finally, it should be stated that y-axis in Figure 11 represents the computational complexity with the millisecond unit, which is the calculation time for every inversion. The actual number may vary in different computers, but the trend will remain almost the same.

IV. EXPERIMENTS IN REAL DATA

A. DATA COLLECTION

With the help of the Civil Aviation Gansu Air Traffic Control Sub Bureau, we collected 24-hour ADS-B messages from

midnight of March 2, 2020, to the next day around Gansu Province in the north-west area of China.

After decoding the ADS-B messages, we apply quality control on the decoded message. Any message with the following conditions will be discarded:

1) Critical items are missing, such as longitude, latitude, report time, geometric height, flight level, ground speed vector, target identification.
2) Any of longitude, latitude, or geometric height is the same as that of the last message, which means duplicate message.

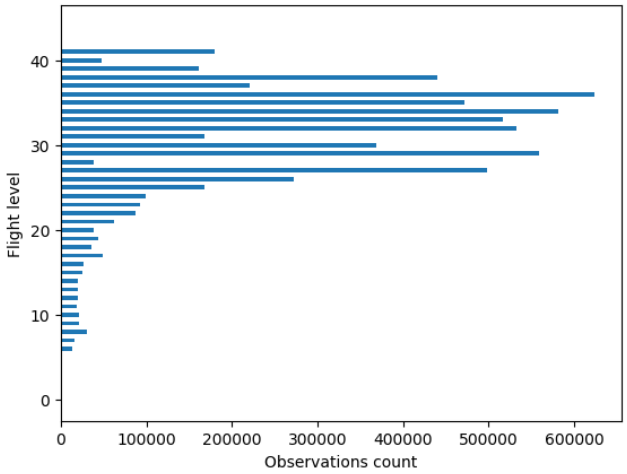

FIGURE 12. Observations statistics among 24 hours grouped by FL. FL is dimensionless, typically ranging from 0 to 410.

After quality control, over 6.5 million valid ground speed vectors are obtained during this period. Figure 12 shows the histogram with the count of raw valid ground speed samples per FL, in which FL is dimensionless. It must be clarified that under FL50, the counts are not zero but small count numbers too small to be recognized in the plot. Vertically, the measurements are mainly concentrated above FL250 in the cruising phase.

Grouping by the target identification item, there are about 1395 trajectories in this spatial-temporal region. Figure 13 illustrates the ground projection of all trajectories. The longitude is ranging from 91°E to 111.6°E, which covers about 200km, and the latitude is ranging from 31.3°N to 42.8°N. The spatial area is about 2100 km^2, covering the whole geographical region of Gansu Province.

Next, we conduct slicing on the 24-hour data streaming with a sliding window of 6 intervals to calculate the track angle difference. Then we can extract turning maneuver slices from them. In total, 2000 turning slices above 5deg were extracted during this period, whose distribution is listed in Table 4, from which wind speed vectors can be calculated. Figure 14 illustrates the turning slices amount distribution on every FL, indicating a large percentage of turning in those high FLs over FL200 or cruising level. Statistically, there is a large percentage of turning slices with smaller angle, so it

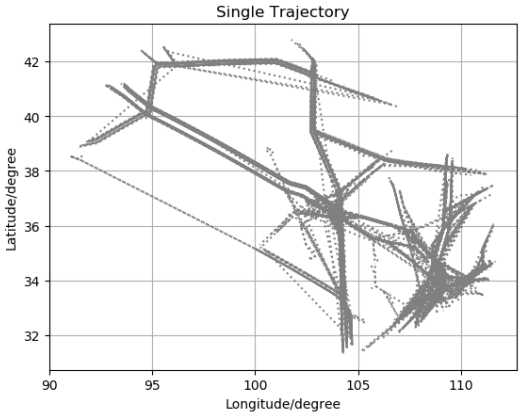

FIGURE 13. Ground projection of trajectories.

TABLE 4. Turning angle distribution group by flight level.

FL	<20°	20°-30°	30°-40°	40°-50°	>50°
0-100	4	9	4	7	48
100-200	71	28	28	15	53
200-300	335	88	60	36	46
300-400	796	115	58	41	114
>400	38	2	1	2	1
	62.20%	12.10%	7.55%	5.05%	13.10%

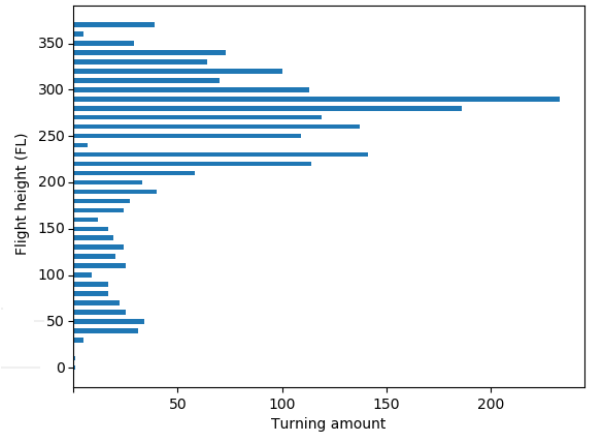

FIGURE 14. Turning slices amount distribution with FL.

is essential to explore algorithms suitable for the small-angle turning.

B. LARGE ANGLE TURNING EXPERIMENT

In this experiment, we selected slices with the large turning angles above 40deg and compared the performance of three algorithms, as shown in Figure 15. Subplots in the same row are calculated from the same slice. Subplots in the left column are processed by LM, middle by LS, right by STD. Here we can find that in large angle situations, all three algorithms

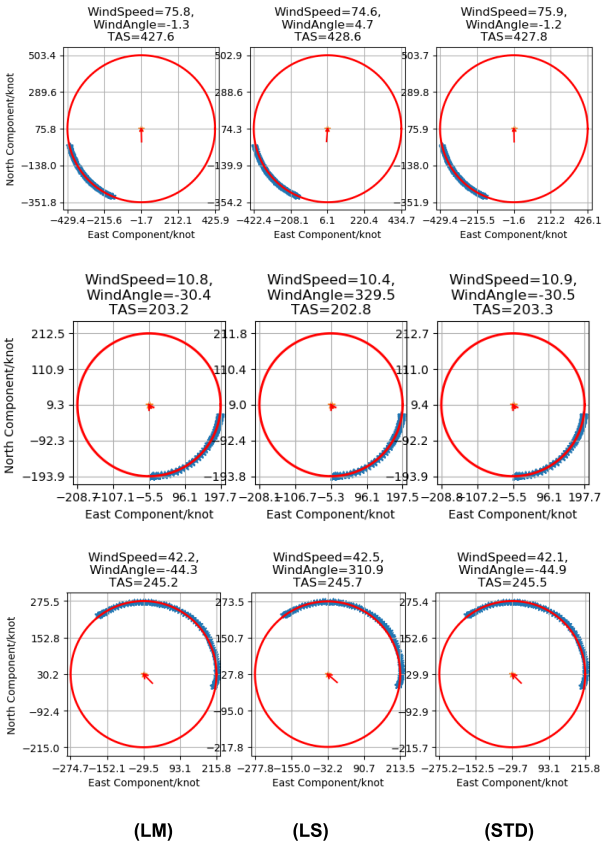

FIGURE 15. Fitting circles in state space with large turning angle.

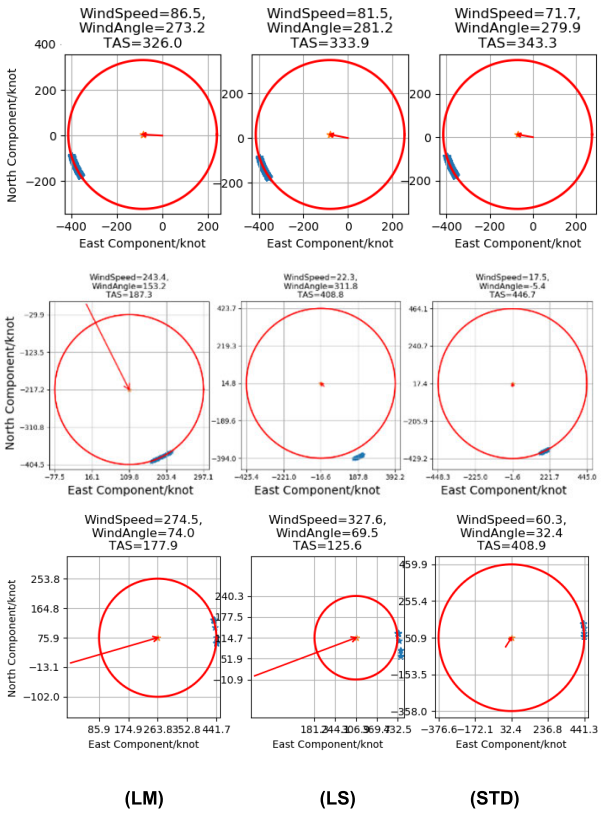

FIGURE 16. Fitting circles in state space with small turning angles.

work well and can obtain almost identical results. Both wind speed and TAS in these results have a high confidence level, being consistent with the possible wind speed range.

TABLE 5. MAE of wind speed, wind direction and TAS for three algorithms, when turning >40deg.

MAE (deg/knot)	Wind speed	Wind direction	TAS
< 2	68.56%	63.66%	64.62%
< 3	74.74%	75.26%	71.74%
< 4	77.84%	81.19%	76.41%
< 5	80.15%	83.25%	79.12%
< 6	80.93%	84.28%	79.85%
< 7	82.47%	84.79%	81.08%
< 8	84.28%	85.82%	82.80%
< 9	85.05%	86.08%	84.03%

Furthermore, MAEs of estimates are calculated for three algorithms to verify the stability of results, as listed in Table 5. Totally, there are 388 slices over 40deg. In terms of wind speed, 68.6% slices have MAE under 2 knots, and 85% under 9 knots. For wind direction, 63.7% slices have MAE under 2deg and 86.1% under 9deg. For TAS, 64.6% have MAE under 2 knots and 84.0% under 9knots. The experiment results show that all three algorithms have stable and close performance in the case of large angle turning maneuvers.

C. SMALL TURNING ANGLE EXPERIMENT

In this experiment, we selected slices with turning less than 40deg, and compared the performance of three algorithms, as shown below in Figure 16, where the left column corresponds to LM, the middle column LS, the right column STD.

The first row illustrates in one example that three algorithms have closer and satisfactory fitting results on wind speed and TAS estimate. Around 330 knots, TAS and 80 knots wind speed are among the empirical TAS values with a high confidence level.

In the second row, LM gives an abnormal result, noticing that the estimate of the wind speed 243.4knot and TAS estimate 187.3 are unusual with rather a lower probability. Contrastingly, LS and STD have good estimates. TAS of 408.0 knots and 446.7 knots, wind speed of 22.3 knots, and 17.5 are acceptable and close to the typical situation.

In the third row, both LS and LM give out the obviously wrong estimates, because wind speed has a low probability of over 270 knots and TAS under 200 knots. On the contrary, STD obtains a reasonable estimate, as TAS 408.9 knots and wind speed 60.3 knots are typical values in daily aviation. We must notice that all estimates in the right column are

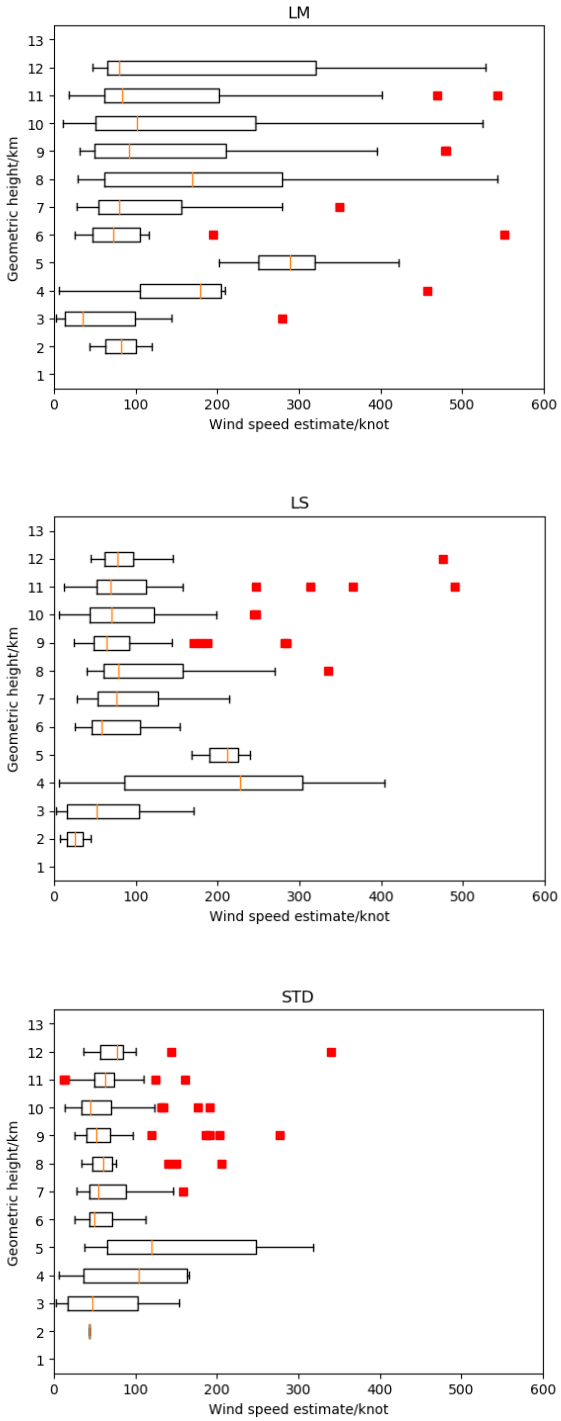

FIGURE 17. Wind speed estimate and comparison grouping by geometric height.

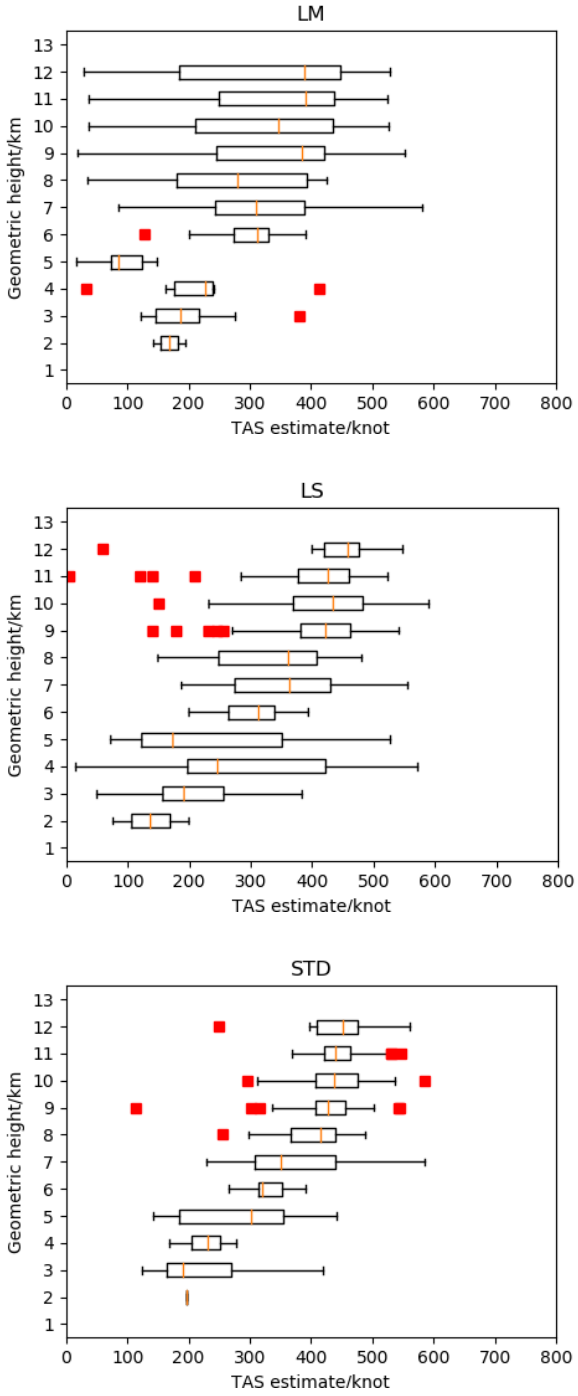

FIGURE 18. TAS estimate and comparison grouping by geometric height.

processed by the STD algorithm, and shown to have higher stability superior to the other two in case of small turning angle situations.

Among turning under 30deg, we found several extreme cases. For instance, we got some wind speed estimates under zero or over 500 knots, which are inacceptable. Further research shows that the occurrence of extreme values strongly relies on the data quality of the turning slice. Because data quality control or data clearance is a tricky and challenging task, we simply discard these extreme values.

D. ONE HOUR EXPERIMENT COMPARISON

In this experiment, we conduct a one-hour experiment from 08:00 to 09:00 AM on March 2, 2020, for the purpose of speed estimate distribution analysis along with the height. Due to the influence of the coronavirus pandemic, starting

at the beginning of this year, there were fewer flights than usual. During this period, around 300 turning slices or wind vector estimates were generated. The statistics of wind speed estimate in different geometric heights are calculated and shown in Figure 17, for LM, LS, and STD, respectively, from top to bottom.

In LM and LS, there are many wind speed estimates greater than 200 knots. According to the real situation and empirical data, this is of rather low probability. On the contrary, the STD results mainly concentrate on values below 200 knots, which is the rather attractive merit superior to the other two. Notably, the concentration above 6km height for STD is rather compact and obvious in the three figures.

Next, we conduct statistics for TAS estimates in different geometric heights, as illustrated in Figure 18. It must be remembered that the TAS is almost equal to the ground speed with little bias, and the typical flight speed is around 300-500 knots. In LM and LS, there are a lot of TAS estimates with low values less than 300 knots above 6km geometric height. These speed values are rather rare in real flight situations. Besides, the data concentration degree in every height is rather unsatisfactory. On the contrary, TAS has a better concentration in every height than the other two, and the trend that speeds escalating with the height going-up is rather apparent, which is an attractive advantage superior to the other two. Furthermore, speed values above 6km mainly concentrate between 300 and 500 knots, which agrees well with the real situation and empirical values.

V. CONCLUSION

In this article, the speed vector model is introduced, and under the hypotheses that wind vector and TAS remain constant, the simplified model is also introduced. Next, we describe the wind speed vector inversion algorithms, specifically the LS proposed by Hurter *et al.* [22], the LM by Leege *et al.* [19], and our novel STD method.

Based on the simulation test, three algorithms are compared. The wind speed and direction estimates are negatively affected by the TAS standard deviation. If 95% of the aircraft airspeed vary within 15 knots, the MAE of 1-4kt and 1-5deg for the wind speed and direction estimates are expected, respectively. The MAE of the wind speed estimate is uncorrelated with the actual wind speed for LS and STD algorithms. The MAE of the wind direction estimate is negatively correlated with the actual wind speed with p <0.01. The geometric shape or the turning angle has a positive influence on the MAE performance. Three algorithms will converge to satisfactory MAE of wind speed under 0.5 knots if the turning increases to a large enough angle, 220deg. Under 20deg, LS has performance too unsatisfactory to apply in a real situation, but the STD results in very low MAE, superior to other two algorithms. This merit can further increase data availability. The computational complexity comparison shows that LS remains the lowest and almost changeless with the data amount, STD in between, and LM the highest.

Furthermore, based on real ADS-B data, three algorithms work well in the case of the large turning situation over 40deg and have consistent results with higher confidence levels. Nevertheless, in smaller turning under 40deg, LS and LM do not always work well, sometimes give noticeable incorrect results or extreme values. Comparably, our proposed STD works well in small turning. STD has a better estimate concentration level than the other two methods. This merit can help improve the data utilization for the next wind field reconstruction.

Consequently, this article verifies the feasibility of wind speed vector inversion methods based on ADS-B data, and proposes a novel standard derivation based algorithm to improve the performance in the situations of small-angle turning maneuver, which is regarded as the fundamental research for next spatial-temporal wind flow field reconstruction.

The research direction after this article will aim at: 1) improving STD algorithm stability against noise and slice uncertainty; 2) wind flow field reconstruction model; 3) comparison to wind field estimate from GRAPSE numeric weather forecast model; 4) short-time forecasting for wind field; 5) complicated system and ADS-B data network, data fusing with SSR system; 6) ADS-B data sharing platform similar to AMDAR.

REFERENCES

[1] J. Xie, H. Sun, Y. Jiao, and B. Lu, "Association rules mining with QAR data: An analysis on unstable approaches," in *Proc. IEEE 1st Int. Conf. Civil Aviation Saf. Inf. Technol. (ICCASIT)*, Oct. 2019, pp. 603–606.

[2] Y. Xinrui, W. Lei, and L. Ruiyi, "Data quality evaluation of chinese wind profile radar network in 2018," in *Proc. Int. Conf. Meteorol. Observat. (ICMO)*, Dec. 2019, pp. 1–4.

[3] S. Ishii, K. Okamoto, P. Baron, T. Ishibashi, T. Tanaka, T. Sekiyama, T. Maki, T. Kubota, Y. Satoh, D. Sakaizawa, K. Yamashita, K. Gamo, S. Ochiai, M. Yasui, R. Oki, M. Satoh, and T. Iwasaki, "Study on measurement performance of future space-based Doppler wind lidar in japan," in *Proc. IEEE Int. Geosci. Remote Sens. Symp. (IGARSS)*, Jul. 2017, pp. 4238–4245.

[4] T. Naakka, T. Nygård, M. Tjernström, T. Vihma, R. Pirazzini, and I. M. Brooks, "The impact of radiosounding observations on numerical weather prediction analyses in the arctic," *Geophys. Res. Lett.*, vol. 46, no. 14, p. 46, 2019.

[5] H. Wang, N. Shao, and Y. Ran, "Identification of precipitation-clouds based on the dual-polarization Doppler weather radar echoes using deep–learning method," *IEEE Access*, vol. 7, pp. 12822–12831, 2019.

[6] L. Tao, L. Wei, Q. Hua, and X. Zhili, "Wind vector inversion method of based on ADS-B data," *J. Chengdu Univ. Inf. Technol.*, to be published.

[7] (Aug. 2018). *Automatic Dependent Surveillance-Broadcast (ADS-B)*. [Online]. Available: https://www.faa.gov/nextgen/programs/adsb/

[8] D. Primo, F. Escobar, D. Badino, and J. R. Vittar, "System acquisition, processing and visualitation of air traffic using ADS-B and IoT connectivity," in *Proc. IEEE Biennial Congr. Argentina (ARGENCON)*, Jun. 2018, pp. 1–5.

[9] B. Syd Ali, W. Schuster, W. Ochieng, and A. Majumdar, "Analysis of anomalies in ADS-B and its GPS data," *GPS Solutions*, vol. 20, no. 3, pp. 429–438, Jul. 2016.

[10] M. Angelilli, L. Infante, and P. Pacifici, "A family of secondary surveillance radars based on conformal antenna array geometries," in *Proc. IEEE Radar Conf. (RadarConf)*, May 2017, pp. 1681–1684.

[11] E. A. Suteja, A. D. Prasetyo, B. Satriyotomo, D. H. Dafiq, and Edwar, "ADS-B microstrip antenna receiver design for cubesat with slot," in *Proc. Int. Conf. Inf. Commun. Technol. (ICOIACT)*, Jul. 2019, pp. 17–21.

[12] P. Ren, J. Wang, H. Song, P. Zhang, and T. Ban, "A novel multi-criteria preamble detection algorithm for ADS-B signals," *IEEE Access*, vol. 7, pp. 97319–97332, 2019.

[13] S. Chen, S. Zheng, L. Yang, and X. Yang, "Deep learning for large-scale real-world ACARS and ADS-B radio signal classification," *IEEE Access*, vol. 7, pp. 89256–89264, 2019.
[14] N. M. S. Iswari and I. M. Astawa, "Development of human-machine interface system for flight monitoring using ADS-B data and openmap," in *Proc. Joint 10th Int. Conf. Soft Comput. Intell. Syst. (SCIS) 19th Int. Symp. Adv. Intell. Syst. (ISIS)*, Dec. 2018, pp. 518–523.
[15] H.-W. Peng and S.-S. Jan, "Development of a three-dimensional aviation unusual weather detection system based on the use of ADS-B 1090MHz data," in *Proc. Int. Tech. Meeting Inst. Navigat.*, Feb. 2016, pp. 564–572.
[16] W. M. Hollister, E. R. Bradford, and J. D. Welch, "Using aircraft radar tracks to estimate wind aloft," *Lincoln Lab. J.*, vol. 2, no. 3, pp. 555–565, 1989.
[17] D. Delahaye and S. Puechmorel, "TAS and wind estimation from radar data," in *Proc. IEEE/AIAA 28th Digit. Avionics Syst. Conf.*, Oct. 2009, pp. 2. B. 5-1–2. B. 5-16.
[18] S. D. Haan, M. D. Haij, and J. Sondij, "The use of a commercial ADS-B receiver to derive upper air wind and temperature observations from Mode-S EHS information in The Netherlands," KNMI, De Bilt, Germany, Tech. Rep., TR-336, 2013.
[19] A. M. P. de Leege, M. M. van Paassen, and M. Mulder, "Using automatic dependent surveillance-broadcast for meteorological monitoring," *J. Aircr.*, vol. 50, no. 1, pp. 249–261, Jan. 2013.
[20] G.-J. Liou and S.-S. Jan, "Using on air UAT/ADS-B signal to simulate 3D aviation weather information," in *Proc. IEEE/ION Position, Location Navigat. Symp. PLANS*, May 2014, pp. 671–679.
[21] A. Kapoor, Z. Horvitz, S. Laube, and E. Horvitz, "Airplanes aloft as a sensor network for wind forecasting," in *Proc. IPSN-14 Proc. 13th Int. Symp. Inf. Process. Sensor Netw.*, Apr. 2014, pp. 25–33.
[22] C. Hurter, R. Alligier, D. Gianazza, S. Puechmorel, G. Andrienko, and N. Andrienko, "Wind parameters extraction from aircraft trajectories," *Comput., Environ. Urban Syst.*, vol. 47, pp. 28–43, Sep. 2014.
[23] W.-Y. TING and S.-S. Jan, "Development of an aviation unusual weather now-casting system based on aircraft automatic dependent surveillance-broadcast (ADS-B) data," in *Proc. 18th Conf. Aviation, Range, Aerosp. Meteorol.*, Seattle, WA, USA, Jan. 2017, pp. 1–4.
[24] S. Junzi, H. Vû, J. Ellerbroek, and J. M. Hoekstra, "Weather field reconstruction using aircraft surveillance data and a novel meteo-particle model," *PLoS ONE*, vol. 13, no. 10, 2018, Art. no. e0205029.
[25] J. Sun, H. Vu, J. Ellerbroek, and J. Hoekstra, "Ground-based wind field construction from mode-S and ADS-B data with a novel gas particle model," in *Proc. 7th SESAR Innov. Days*, Belgrade, Serbia, 2017, pp. 1–9.
[26] V. Huy, "ADS-B and mode-S data for aviation meteorology and aircraft performance modelling," M.S. thesis, Fac. Aerosp. Eng., Delft Univ. Technol., Delft, The Netherlands, 2018.
[27] M. Schafer, M. Strohmeier, M. Smith, M. Fuchs, R. Pinheiro, V. Lenders, and I. Martinovic, "OpenSky report 2016: Facts and figures on SSR mode s and ADS-B usage," in *Proc. IEEE/AIAA 35th Digit. Avionics Syst. Conf. (DASC)*, Sep. 2016, pp. 1–9.
[28] M. Schafer, M. Strohmeier, M. Smith, M. Fuchs, V. Lenders, M. Liechti, and I. Martinovic, "OpenSky report 2017: Mode s and ADS-B usage of military and other state aircraft," in *Proc. IEEE/AIAA 36th Digit. Avionics Syst. Conf. (DASC)*, Sep. 2017, pp. 1–10.
[29] M. Schafer, M. Strohmeicr, M. Smith, M. Fuchs, V. Lenders, and I. Martinovic, "OpenSky report 2018: Assessing the integrity of crowd-sourced mode s and ADS-B data," in *Proc. IEEE/AIAA 37th Digit. Avionics Syst. Conf. (DASC)*, Sep. 2018, pp. 1–9.
[30] (Mar. 8, 2018.). *CAT021—EUROCONTROL Specification for Surveillance Data Exchange ASTERIX Part 12 Category 21 (Appendix A) Version 1.4*. [Online]. Available: https://www.eurocontrol.int/publication/cat021-eurocontrol-specification-surveillance-data-exchange-asterix-part-12-category-0
[31] T. Liu and Z. Li, "Particle filter based wind vector inversion for ADS-B data," in *Proc. 3rd ICMMI Int. Workshop Electr. Electron. Eng. (IWEEE)*, Mumbai, India, Apr. 2020, p. 256.
[32] P. M. A. de Jong, J. J. V. D. Laan, A. C. 'tVeld, M. M. van Paassen, and M. Mulder, "Wind-profile estimation using airborne sensors," *J. Aircr.*, vol. 51, no. 6, pp. 1852–1863, Nov. 2014.

TAO LIU was born in Guizhou, China, in 1977. He received the B.S. and M.S. degrees in control theory and engineering from Chongqing University, Chongqing, China, in 2000 and 2003, respectively, and the Ph.D. degree in signal and information processing from the University of Electronic Science and Technology of China, Chengdu, Sichuan, China, in 2009. From 2016 to 2017, he was supported by the Western China Talented Personnel Promotion Project of the China Scholarship Council to work as a Visiting Scholar with the University of Florida, Gainesville, FL, USA. He is currently a Teacher with the School of Electronic Engineering, Chengdu University of Information Technology. He has authored one book, more than 20 articles, and three patents. His research interests include meteorological satellite remote sensing signal processing, radar signal processing, image processing, artificial intelligence, and software design.

TAISONG XIONG was born in China, in 1976. He received the B.S., M.S., and Ph.D. degrees in the School of Computer Science and Engineering, UESTC, Chengdu, China, in 2000, 2006, and 2013, respectively. Since 2013, he has been a Teacher with the School of Applied Mathematics, Chengdu University of Information Technology. His research interests include machine learning and image processing.

LENWORTH THOMAS was born in Orlando, FL, USA, in 2000. He is currently pursuing the bachelor's degree in mechanical engineering with the University of Florida. As a recent McNair Scholar Award recipient, he has been conducting research on small-scale LiDAR systems. Using his passion for cutting-edge robotics and his research experience, he hopes to pursue the Ph.D. degree at a top university after he graduates.

YONGLOU LIANG was born in China, in 1979. He received the bachelor's degree in computer science and technology from the Huazhong University of Science and Technology, in 2004. He has been employed and working with Beijing Huayun Shinetek Science and Technology Company, since 2005. For more than a decade, he has devoted to relevant research and data application in remote sensing area for users within China region and global range and has successfully arranged establishment of more than 200 satellite data receiving and utilization ground stations covering geostationary and polar-orbiting satellites of different generations, providing data source of good stability for both domestic and international users of different application areas, including weather forecast and academic research.